RSC Advances

ROYAL SOCIETY OF CHEMISTRY

www.rsc.org/advances

Friction of aromatic thiol monolayers on silver: SFA and AFM studies of adhesive and non-adhesive contacts

Y. Yang[a], J. Singh[b], and M. Ruths*

Department of Chemistry, University of Massachusetts Lowell,
1 University Avenue, Lowell, MA 01854, USA

* author to whom correspondence should be addressed.
Email: marina_ruths@uml.edu

a) current affiliation: Lubrizol Advanced Materials, Inc., Brecksville, OH 44141.
Email: yutao.yang@lubrizol.com

b) current affiliation: domnick hunter Process Filtration, Oxnard, CA 93030.
Email: jagdeep.singh@parker.com

ABSTRACT

The boundary friction of aromatic thiol (thiophenol, *p*-phenylthiophenol, and *p*-terphenylthiol) and octadecanethiol self-assembled monolayers on template-stripped silver was measured under adhesive and non-adhesive conditions with the Surface Forces Apparatus (SFA) and Atomic Force Microscopy (AFM). In non-adhesive contacts, the friction force increased linearly with load. Friction coefficients obtained with the two techniques were in good agreement and decreased with increasing packing density of the aromatic monolayers, but did not reach the low value obtained for octadecanethiol. The sublinear increase in friction force vs. load in adhesive contacts was evaluated as critical shear stresses based on nominal contact areas directly measured with the SFA and calculated using the Thin-Coating Contact Mechanics model for the AFM. The same trend was found in the shear stresses as in the friction coefficients.

INTRODUCTION

Friction and lubrication are complex processes where very different responses can be obtained through slight variations of materials and conditions. The fields of nano- and microtribology have been developed to provide a fundamental understanding of friction at the molecular, nanoscopic, and microscopic length scales, with the expectation that macroscopic friction phenomena may eventually be explained and predicted based on this knowledge. In boundary friction, which involves bare or monolayer-covered surfaces in "dry" contact or separated by fluid-like films with a thickness of a few molecular diameters,[1] it is known that the chemical properties (molecular structure, conformation, order, interaction, and reactivity) of the surfaces and films and the topology (at the molecular, nanoscopic, and microscopic length scales) play important roles. These parameters can be explored by direct friction force measurements using the Surface Forces Apparatus (SFA) and Atomic Force Microscopy (AFM).

The interacting surfaces in the SFA and AFM are typically assumed to form a "single-asperity" contact, where the area of contact is the nominal one between a perfectly smooth sphere and a flat surface. The friction force, F, measured with these techniques at low loads, L, in an adhesive contact between surfaces that can be considered "atomically smooth" (mica or other crystalline substrates) or slightly rough at the molecular level (e.g., self-assembled monolayers of different packing density) has been observed to increase sub-linearly with L,[1–12] in proportion to the nominal contact area, A ("adhesion-controlled" friction), and thus showing an apparent dependence on the radius of curvature, R, of the SFA surfaces or AFM tip in a manner predicted by contact mechanics models for macroscopic bodies.[13–15] In contrast, surfaces with no or very low adhesion have shown a linear dependence of F on L with no apparent dependence on R ("load-controlled" friction).[6–12,16–20]

These friction responses are not fully explained, although they have been observed for decades and key aspects of them can be reproduced in computer models. Recent computer simulations[21–23] have suggested that within the nominal contact area, the size of the real, molecular contact area as well as its increase with increasing load are

adhesion-dependent, but in a different manner than that observed for nominal or macroscopic contacts.[13–15] Molecular scale roughness, real contact areas, and changes therein are difficult to quantify in nanoscale friction experiments, which involve deformable substrates in continuous motion under considerable pressure. In contrast, the nominal contact area can be either directly measured (in the SFA) or estimated from contact mechanics models (for the AFM), although concerns have been raised about the applicability of such models on the nanometer and sub-nanometer scale[24] where atomic level roughness causes local changes in the pressure. This influence of the substrate structure was reduced but not removed when a molecularly thin film was present in the contact.[23]

Here, investigations of the adhesion and load contributions in different systems with roughness at the atomic and molecular levels were extended from nanometer-sized contacts in the AFM to larger areas in the SFA. In the SFA, where the radius of curvature of the surfaces is 5–6 orders of magnitude larger than in the AFM, the nominal contact area is 3–4 orders of magnitude larger and the friction response is thus an average over many more molecules than in the AFM. Aromatic thiol self-assembled monolayers (SAMs) and a close-packed alkanethiol SAM were chosen as model systems to further explore the effects of molecular structure and monolayer packing density and rigidity.[25–28] The monolayers were formed on template-stripped silver in order to utilize the optical interferometry technique available for measurements of R and A in the SFA. The adhesion was modified by immersing the contacts in either dry N_2 gas or ethanol to obtain van der Waals interactions of different magnitude between the surfaces. Previous work has indicated that ethanol does not remain confined between the surfaces under the chosen conditions,[8–10] but some penetration of ethanol into poorly packed monolayers cannot be excluded.

Friction data were acquired in adhesive and in non-adhesive contacts with both techniques, building on previous work involving only one technique or one condition, such as comparing different surface or tip radii or different adhesion strengths within one technique,[6–12,16,19] or comparison of AFM and SFA data obtained under non-adhesive

conditions (linear friction) only.[18] The observed sub-linear and linear F vs. L in adhesive and non-adhesive systems, respectively, were in agreement with the responses predicted by computer simulations of real contact areas.[21–23] A good agreement was found between friction coefficients measured with SFA and AFM in non-adhesive contacts. The friction of the aromatic SAMs decreased with increasing packing density but was significantly higher than that of the alkanethiol. The same trend was seen under adhesive conditions in the critical shear stresses calculated from F values obtained with both techniques and the corresponding nominal contact areas A.

MATERIALS AND METHODS

SELF-ASSEMBLED MONOLAYERS ON SILVER

Aromatic and polyaromatic thiols are known to form self-assembled monolayers (SAMs) on silver,[29–35] although less information is available on the resulting structures than on those formed on gold (cf. ref. 9 and references therein). Schematic molecular structures of the compounds investigated here, thiophenol (TP, Fluka, purity 99.6%), *p*-phenylthiophenol (PTP, Oakwood Products, West Columbia, SC, 97%), and *p*-terphenyl thiol (TPT, Frinton Laboratories, Vineland, NJ), are shown in Scheme 1.

Scheme 1. Aromatic thiols

Thiophenol (TP) Phenylthiophenol (PTP) Terphenylthiol (TPT)

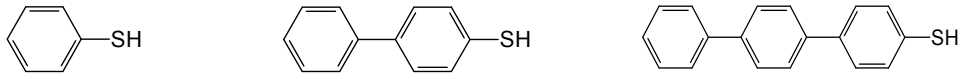

For the AFM experiments, monolayers of these thiols and of 1-octadecanethiol (ODT, Sigma-Aldrich, 98%) were formed by immersing template-stripped silver substrates overnight in ethanol (Sigma – Aldrich, ≥99.5%) solutions with the concentrations given in Table 1. The 50 nm thick template-stripped silver was prepared analogously to template-stripped gold substrates in ref. 9, i.e., by letting the silvered side of a mica sheet adhere to heated polystyrene, allowing the resulting assembly to cool, and removing the

mica right before immersing the substrate in thiol solution. The extent of possible oxidation of the freshly exposed template-stripped silver (previously in contact with the mica) while transferring the substrate into solution was not explored in this study, and no differences were observed in the contact angles or friction of monolayers on substrates prepared from silver evaporated the same day or months earlier, provided that the exposure to laboratory air was brief after removing the mica. For the SFA measurements, the template-stripped silver was formed on a half-cylindrical quartz-glass support by gluing the silvered side of a mica sheet down with Norland Optical Adhesive #61, cured with a Pen-Ray lamp (18 W) at a distance of about 2 cm for 1.5 h. This glue does not dissolve and shows minimal swelling when immersed in ethanol during the self-assembly. The opposing surface in the SFA measurements was a bare (unmodified), back-silvered mica surface, whereas in the AFM experiments it was a Si tip (CSC17, MikroMasch) covered with a layer of native oxide.

Table 1. Properties of SAMs on silver. Solution concentration, monolayer thickness *h*, molecular area, and tilt angle from surface normal.

SAM	***Conc.*** **(mM)**	***h*** **(nm)**	***Molec. area*** **(nm^2)**	θ_{tilt} **(°)**
TP	0.8–1.0	0.6 [31] 0.7 [33]	0.305 [29] 0.328 [30]	24 [31] 29 [29] 37 [32]
PTP	0.5–0.6	1.1 [31] 1.3 [33]	0.27 [a]	18 [35] 0–10 [34]
TPT	0.03–0.05	1.5 [31] 1.7 [35]	0.24 [a]	16 [31]
ODT	1.0	2.41 [36]	0.2175 [36] 0.195 [37]	12 [36]

[a]Estimated from the S_{2p}/Ag_{3d} ratio measured by XPS and the average molecular area of ODT.

Some information on monolayer thicknesses *h*, molecular areas and tilt angles on silver can be found in the literature (cf. Table 1), and averages of these values of *h* were used in the contact mechanics model described below. TP is known to form a poorly packed monolayer on gold, whereas PTP and TPT form more close-packed, rigid layers with their molecules in a nearly upright orientation, and qualitative statements in the literature suggest that a similar behavior is expected on silver although values of the molecular area were found only for TP (Table 1). The molecular areas of PTP and TPT on silver were estimated by using X-ray photoelectron spectroscopy (XPS, VG ESCALAB MKII, Mg Kα X-ray, 200 W). Spectra of the SAMs (PTP, TPT and, for comparison, 1-octadecanethiol) on silver were obtained, referenced to C(1s) = 284.6 eV. From the spectra, the sulfur to silver ratio (S_{2p}/Ag_{3d}) was calculated: 1-octadecanethiol (0.093), PTP (0.072), and TPT (0.081). Based on the reported molecular area [36,37] of 1-octadecanethiol, (an average value of 0.21 nm^2/molecule, cf. Table 1), the molecular areas of PTP and TPT on Ag were estimated proportionally: PTP (0.27 nm^2), TPT (0.24 nm^2). These values are smaller than the literature values for TP (Table 1), which is consistent with the expected more close-packed structure of the PTP and TPT monolayers. For comparison, the area occupied by a vertically oriented benzene ring is 0.21 nm^2, based on van der Waals and covalent radii.[38,39]

CONTACT ANGLES AND SURFACE ENERGIES

A Krüss Drop Shape Analysis System 100 (Germany) was used to measure the advancing and receding contact angles of distilled water, and the advancing contact angles of methyl iodide (MI), on the aromatic SAMs (Table 2). The uncertainty in the measurement is about 1°. The values in Table 2 are averages of 2–5 measurements at different positions on several separately prepared samples. The corresponding experimental values of the surface energies, γ_{YD}, were calculated using the Young–Dupré equation (cf. Supplementary Information).[40,41] The values of $\gamma_{YD} = \gamma_S^p + \gamma_S^d$, where γ_S^p and γ_S^d are the polar and dispersive contributions to the surface energy of the solid, respectively, are given in Table 2, and were around 38 mJ/m^2 (for ODT, γ_{YD} = 27 mJ/m^2). γ_S^p is quite low in all the aromatic systems, i.e., the surface energy of the SAMs arises mainly from

dispersive intermolecular interactions as noted previously for monolayers of these compounds and phenyl terminated alkanethiols on gold.[9,10]

These values can be compared to theoretical surface energies, $\gamma_{vdW} = A_H/(24\pi D_0)^2$, (Table 2) at a cut-off distance D_0 = 0.165 nm.[40] The Hamaker constant A_H was calculated according to the van der Waals–Lifshitz theory for a symmetrical three-layer system[40] SAM/dry N_2 gas/SAM, with bulk refractive index and dielectric constant 1.59 and 4.26 for TP, 1.55 and 4.5 for PTP, and 1.55 and 4.2 for TPT (using the corresponding values for ODT, 1.47 and 2.2, one obtains γ_{vdW} = 31 mJ/m^2). A similar approach can be used to calculate the theoretical *interfacial* energy in three-layer asymmetric systems, SAM/dry N_2 gas or ethanol/mica or SiO_2. Such interfacial energies are relevant for comparison with the work of adhesion from the pull-off regime in the friction experiments. The bulk refractive index and dielectric constant 1.6 and 7 for mica and 1.45 and 3.8 for SiO_2 were used to calculate the theoretical interfacial energy in dry N_2 and in ethanol. These values are given in Table 3 in connection with the discussion of the experimental values.

Table 2. Contact angles of water and methyl iodide (MI), experimental Young–Dupré surface energy $\gamma_{YD} = \gamma_S^p + \gamma_S^d$, and theoretical van der Waals–Lifshitz surface energy γ_{vdW}

SAM	θ_{adv,H_2O} (°)	θ_{rec,H_2O} (°)	$\theta_{adv,MI}$ (°)	γ_S^p (mJ/m^2)	γ_S^d (mJ/m^2)	γ_{YD} (mJ/m^2)	γ_{vdW} (mJ/m^2)
TP	82	77	41	3.6	35.9	39.5	46
PTP	94	74	44	0.6	37.4	38	41
TPT	92	74	44	1.0	36.5	37.5	41

FRICTION MEASUREMENTS WITH SFA

In the SFA,[42] normal forces (load, L) and lateral forces (friction force, F) are measured between two macroscopic surfaces placed in a crossed-cylinder configuration, which at small separations is equivalent to the geometry of a sphere near a flat surface. The surfaces form an optical interferometer that permits the determination of gap thickness

(film thickness)[43] between the facing surfaces with an accuracy of 0.1–0.2 nm. The interference fringe pattern is observed in two perpendicular directions for measurements of the radius of curvature of the surfaces, R, with an accuracy of about 10% (R is typically a few cm). In a similar manner, the diameter of a flattened contact region (for example, surfaces in adhesive or compressive contact during a friction measurement) can be measured with an accuracy of 1–2 μm. This diameter is typically 10–200 μm, depending on the strength of adhesion, applied normal force (load), and deformability of the surfaces and glue layers supporting them. The nominal area of contact between the surfaces is therefore typically found in the range 100–30,000 μm^2, in good agreement with predictions from contact mechanics models for interacting bulk or layered materials.[13,44]

In these experiments, we used an SFA3[45] with sliding attachments as described in detail in ref. 46. Compressive or tensile loads were measured and regulated by moving the base of a double cantilever leaf spring (supporting the lower surface) vertically with mechanical stages and detecting its deflection. The spring had a spring constant of 340 N/m, giving a sensitivity in L of about ca. 5×10^{-8} N, To induce sliding, this lower surface was moved laterally back and forth over a distance of 10–20 μm at a constant velocity of v = 1.6 or 3.2 μm/s using a piezoelectric bimorph device.[46] The upper surface was mounted on a friction device, on strain gauge-equipped springs (spring constant 650 or 2400 N/m) whose deflection was proportional to the lateral force between the surfaces (sensitivity in F of a few μN). In cases of very high friction (in the experiments in N_2), the range of linear motion of the bimorph device was too small to induce sliding of the surfaces. Then the friction device was used as both an actuator (using a DC motor) and a detector in back-and-forth sliding over a distance of 100–200 μm at a constant speed chosen in the range 3–6 μm/s. No dependence of the friction force on the sliding velocity was detected in the investigated range.

After mounting the surfaces in the instrument chamber, it was purged with N_2 for a few hours to remove water vapor which would otherwise capillary condense when the surfaces were brought into contact. During experiments in dry N_2 gas, the chamber was

kept dry with P_2O_5 in a salt boat inserted through its wall. For experiments in ethanol (Sigma–Aldrich, ⩾99.5%), a small droplet of ethanol, dried over molecular sieves, was injected between the surfaces through a flush-cleaned PTFE syringe filter (Pall Acrodisc, pore size 0.45 μm). Additional ethanol was placed in the boat (instead of P_2O_5) to decrease the evaporation from the droplet between the surfaces. In some experiments, several contact positions could be found so that measurements were done first in dry N_2 gas and then in ethanol, on the same surfaces but on separate contact positions.

FRICTION MEASUREMENTS WITH AFM

Friction forces, F, were also measured with atomic force microscopy (AFM) in lateral or friction mode, using a Multimode AFM with a Nanoscope IIIa controller (Bruker). The experiments were conducted over a scan length of 1 μm with bare Si tips (CSC17, MikroMasch) carrying a native silicon oxide layer. The scan velocity was 2 μm/s. The dependence of F on velocity was weak in the investigated range (0.4–122 μm/s) and is not reported here. The normal and lateral spring constants were determined from the resonance frequency and quality factor[47, 48] of the cantilevers and from the dimensions[49, 50] as measured by scanning electron microscopy. The normal spring constants were in the range 0.16–0.23 N/m and the lateral spring constants were 20–30 N/m. The geometric mean radius of curvature of the tips, R, was determined by reverse imaging of a calibration sample (TGT01, MikroMasch) at scan angles of 0° and 90°, with an uncertainty of $\Delta R \approx 3$ nm for $R < 100$ nm and $\Delta R \approx 5$ nm for larger tips. The tips used here had radii of 56, 69, 159 and 372 nm.

As in the SFA experiments, the AFM measurements were performed in ethanol (using a fluid cell) and in dry N_2 (in a home-made instrument enclosure). In the experiments in N_2, a relative humidity of ≤ 1.5% (monitored with a Vaisala DM70 dewpoint meter) was reached after purging for 2 h. The statistical error in F (standard deviation of the mean, from averaging the sliding portion of the friction loop) was ca. 0.2 nN at $F < +50$ nN, and 0.5 nN at higher F, and is not shown in Figures 2, 5, and 7 below since it is similar to the height of the symbols. As for the experiments with the SFA, in cases where both

conditions could be explored in the same experiment, the ones in N_2 were done first to reduce the risk of contamination.

CONTACT MECHANICS MODEL

The effective Young's modulus of the mica–glue assembly in the SFA is typically a few tens of GPa.[51] Deformations due to adhesion and compression occur mainly in the glue layer, so that the maximum pressure in the center of the contact is not more than a few tens of MPa. In contrast, the Young's moduli of the AFM tip and substrate, 70–80 GPa for silver, 70–80 GPa for SiO_2,[52] and 170 GPa for Si,[49,50] are much higher than that of a self-assembled monolayer, which is expected to be only a few GPa (cf. Discussion and refs. 9,10). At low L, the radius a of the nominal contact area in the AFM is smaller than or similar to the monolayer thickness h, and the deformations occur mainly within the monolayer. At higher loads, the effective stiffness of such a layered system is still affected by the monolayer and contact mechanics models for homogeneous elastic bodies[13–15] are not expected to apply.

The extended Thin-Coating Contact Mechanics (TCCM) model was used to estimate the nominal contact areas in the AFM experiments on adhesive systems. Measured F values were compared to calculated curves of $F = S_c A$, where S_c was a constant, the critical shear stress, and A was the nominal contact area at a given load L. The details of this model,[53,54] examples of its application to monolayer systems, and evaluations of uncertainties in calculated values are shown elsewhere,[55,56] and only selected information needed for the discussion of the present work is shown here. The probe (a spherical indenter) and the flat substrate are assumed to be rigid, which is a reasonable approximation at low load in our systems. The relationship between L, the radius of the contact area, a, and the work of adhesion ($W = 2\gamma$) in the extended TCCM model is given in non-dimensional form by[53,54]

$$\bar{L} = \frac{\pi}{4}\bar{a}^{4} - \zeta^{1/2}\pi\bar{a}^{2}(2\bar{W})^{1/2} - 2\pi\bar{W}(1-\zeta) \qquad (1)$$

where $\bar{L} = L/(E_u R h)$, $\bar{a} = a/(\sqrt{Rh})$, and $\bar{W} = W/(E_u h)$. The uniaxial strain modulus is

given by $E_u = E(1-\nu)/[(1+\nu)(1-2\nu)]$, where E is Young's modulus, ν is Poisson's ratio (0.4), and h is the film thickness (monolayer thickness in Table 1). $\zeta = 2Wh/E_u\delta_c^2$ is a transition parameter ($0 \le \zeta \le 1$), a measure of the ratio of elastic deformation to the effective range of the surface forces. $\zeta = 0$ and $\zeta = 1$ correspond to limits where the range of adhesion is large and small compared to the elastic deformations. The critical separation, δ_c, was assumed to be 1 nm,[53,54] as in previous applications of this model to monolayer systems.[9,10]

Previous studies of aromatic and aliphatic monolayers[8–10] have indicated that different values of E are needed to describe such systems. Here, E = 7 GPa (E_u = 15 GPa) was used for most of the data on aromatic systems and E = 0.2 or 0.5 GPa (E_u = 0.4 or 1 GPa) for ODT. The uncertainty in S_c mainly arises from propagation of the uncertainties in R, h, E_u, and W in the calculation of A. The uncertainty in S_c can be calculated by differentiating Eq. 1 and using ΔR = 3 nm (R < 100 nm) or 5 nm ($R \ge 100$ nm), Δh = 0.2 nm, ΔE_u = 2 GPa for the aromatic compounds and 0.06 GPa for ODT, and ΔW = 0.002 J/m^2. Following the procedure in ref. 9, the relative uncertainty in S_c in the current experiments was estimated to be about 20% for TP, 13% for PTP and TPT, and 10–13% for ODT.

The net displacement U (here, the indentation into the monolayer) can be calculated from[53,54]

$$\frac{\bar{U}}{\bar{h}} = \frac{\bar{a}^2}{2} - \sqrt{2\zeta\bar{W}} \qquad (2)$$

where $\bar{U} = U/\sqrt{Rh}$ and $\bar{h} = h/\sqrt{Rh}$. Estimates for the monolayer systems (based on the chosen values of E) suggest that at the monolayer transitions observed in the AFM experiments (indicated in Figures 2 and 5), the net displacement in the aromatic systems is 10–15% of the monolayer thickness, which is likely to be beyond the linear elasticity regime assumed in the TCCM model. For ODT it is close to 50% at the transition for R = 69 nm and about 20% for R = 372 nm. In each case, the displacement is approximately half that value at loads half-way between the pull-off and the transition points, which is the region where comparison between the model and the experimental data is of greater interest.

RESULTS

FRICTION AT LOW ADHESION (IN ETHANOL)

Representative results from SFA and AFM measurements performed in ethanol are shown in Figures 1 and 2, respectively. The interfacial energy estimated from the pull-off forces with both techniques was low, $\gamma \leq 2$ mJ/m^2, in all four systems. The sliding velocity v was a few μm/s. The radius of curvature, R, of the surfaces in the SFA was in the range 2–5 cm (R was not measured in all SFA experiments, cf. Supplementary Information) and in the AFM experiments the tip radius was 56–159 nm. A linear dependence of the friction force, F, on load, L, was observed, with $F \rightarrow 0$ when $L \rightarrow 0$. In the AFM experiments (Figure 2), a transition from the reproducible, linear friction force at low loads to a more scattered and less reproducible regime at higher loads occurred at a pressure of about 1–2 GPa, which has been observed previously in monolayer systems at similar pressures.[8–10,18,19] Only the data at low loads, before the transition marked with an arrow in the figures, were included in the linear fit to obtain the friction coefficient μ. Such transitions were not observed in the SFA experiments (Figure 1) because the pressure was lower due to the larger and more deformable substrates.

Values of μ from several SFA and AFM experiments, including the ones shown in Figures 1 and 2, are summarized in Figure 3 and Table 3 (see also Supplementary Information). In Figure 3, μ is shown as a function of molecular area to illustrate the effect of packing density in the aromatic systems. ODT, which has a different molecular structure, was included in the graph for comparison. Except for in the case of TP, where slightly higher μ were obtained with AFM, the values obtained with the two techniques were very similar and showed the trend $\mu_{TP} > \mu_{PTP} \geq \mu_{TPT} > \mu_{ODT}$.

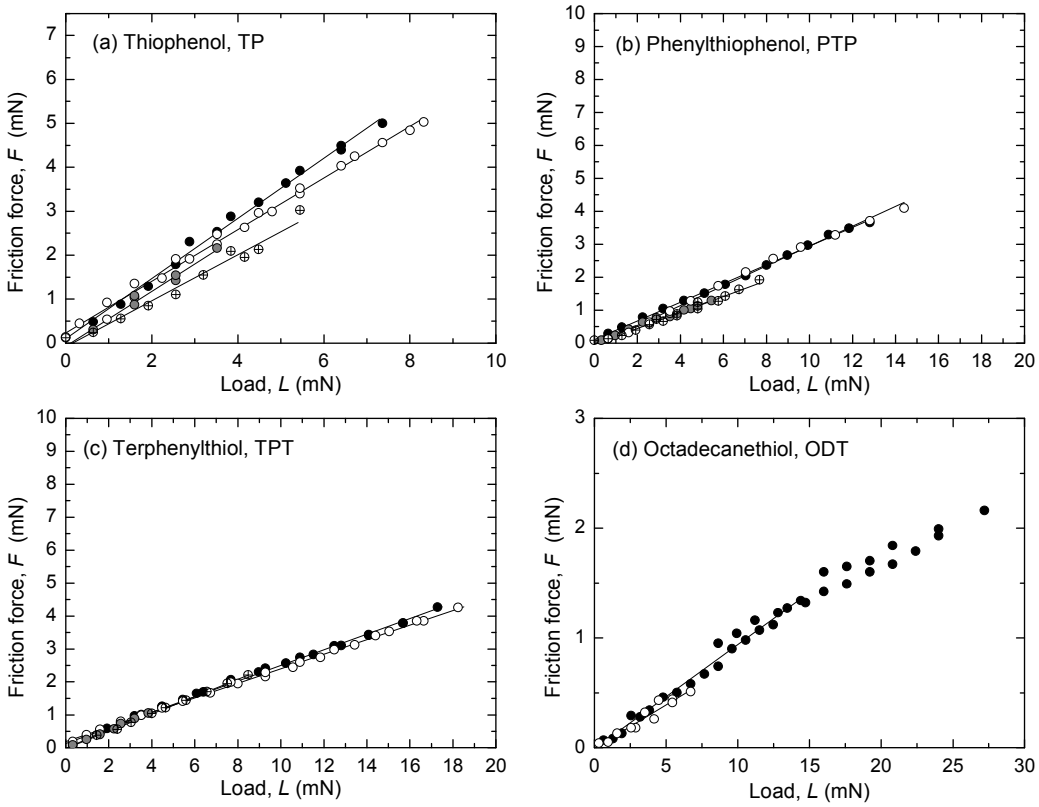

Figure 1. Friction force F vs. load L measured in ethanol with the SFA. The upper disk carried a self-assembled monolayer on template-stripped silver and the bottom surface was bare (unmodified) mica. (a) Thiophenol (TP), (● and ○) v = 3.2 μm/s, R not measured; (gray circle and ⊕) v = 1.6 μm/s, R = 2.53 cm and 4.69 cm. μ = 0.52–0.69. (b) *p*-phenylthiophenol (PTP), (● and ○) v = 3.2 μm/s, R not measured; (gray circle and ⊕) v = 1.6 μm/s, R = 2.57 cm and 4.41 cm. μ = 0.227–0.298. (c) *p*-terphenyl thiol (TPT), (● and ○) v = 3.2 μm/s, R not measured; (gray circle and ⊕) v = 1.6 μm/s, R = 3.13 cm and 2.25 cm. μ = 0.221–0.290. (d) 1-octadecanethiol (ODT), (● and ○) v = 3.2 μm/s, R not measured and R = 2.9 cm. μ = 0.079–0.095. Average μ from these and additional measurements are given in Table 3.

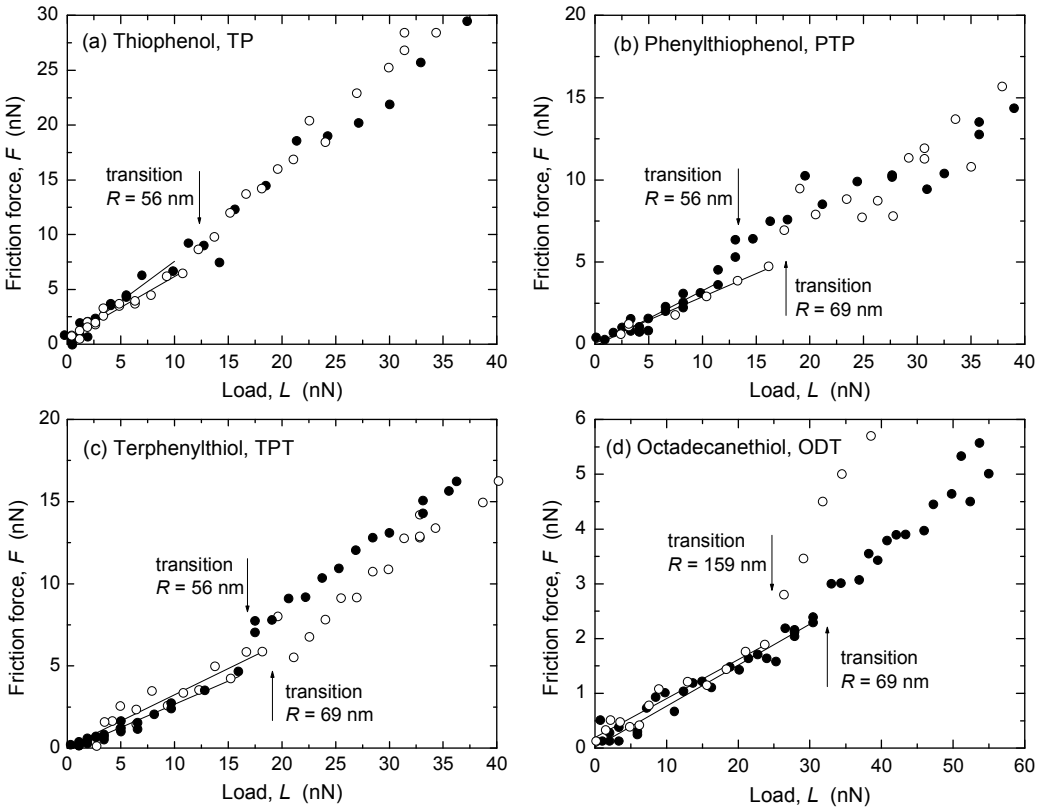

Figure 2. Friction force F vs. load L measured in ethanol with AFM. Scan velocity v = 2 μm/s. (a) TP, (● and ○) two separate experiments with R = 56 nm. μ = 0.56–0.73. (b) PTP, μ = 0.28–0.34, and (c) TPT, μ = 0.28–0.32, (●) R = 56 nm and (○) R = 69 nm in both panels. (d) ODT, (●) R = 69 nm and (○) R = 159 nm. μ = 0.071–0.075. In all systems, the linear low load regime was reproducible, whereas above the transition (marked with an arrow) and up to loads of 100–120 nN (highest loads not shown), the scatter and the differences between different experiments were larger.

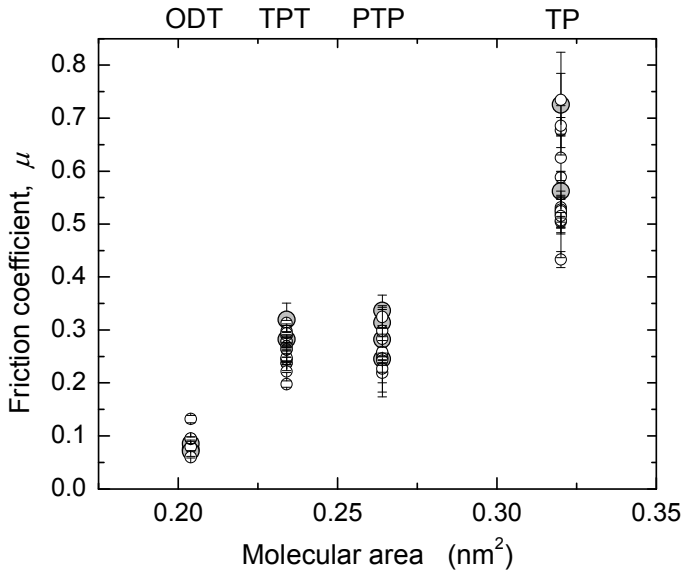

Figure 3. Friction coefficients μ for the four monolayer systems, measured in ethanol with SFA (○) and AFM (larger gray circles).

Table 3. Average friction coefficient μ measured in ethanol and critical shear stress S_c in N_2 gas. Interfacial energy γ_{TCCM} and $\gamma_{vdW,AFM}$, both for interaction across N_2 in the AFM.

System	μ		S_c (MPa)		γ_{TCCM} [a]	$\gamma_{vdW,AFM}$
	SFA	AFM	SFA	AFM	(mJ/m²)	(mJ/m²)
TP	0.56±0.02	0.64±0.08	≥20 (estim.)	683±44 [b]	26±1	36
PTP	0.26±0.01	0.29±0.02	7.3±0.6	385±18 [b]	32±3	34
TPT	0.263±0.007	0.30±0.02	11.5±0.9	465±27 [b]	32±2	34
ODT	0.09±0.01	0.077±0.004	2.9±0.3	20±7 [c] (R = 69 nm) 5.1±1.1 [c] (R = 372 nm)	28±1	30

[a] From the extended TCCM model[53,54], $\gamma_{TCCM} = W/2$.

[b] E = 3–7 GPa, [c] E = 0.2–0.5 GPa.

FRICTION AT HIGHER ADHESION (IN N_2)

The friction forces of the four monolayer systems were also measured in dry N_2 gas (r.h. < 1.5%,) with the SFA (Figure 4) and AFM (Figure 5). In N_2 gas, the adhesion between the surfaces is higher than in ethanol because of the stronger van der Waals forces across dry N_2 than across ethanol. Interfacial energies can be calculated from the measured pull-off forces (and, in the case of the AFM data, from the TCCM model) and compared to values for mica–SAM interaction or silica–SAM interaction expected from van der Waals–Lifshitz theory (Table 3). A good agreement was found. Similarly to in many previous studies of adhesive systems, the values of F and the shape of the F vs. L curves in Figures 4 and 5 were quite different from the data at low adhesion shown in Figures 1 and 2.

In the SFA experiments, the nominal contact area A can be directly measured (cf. inserts in Figure 4) and the critical shear stress S_c directly calculated as F/A. Within experimental uncertainty (note that the relative uncertainty in A is higher than that in F, cf. Materials and Methods), S_c was a constant for each F vs. L curve and reproducible from experiment to experiment. The S_c values from several experiments (cf. Supplementary Information) are shown in Figure 6a and an average for each monolayer system is given in Table 3.

The friction force in the TP system was very high and the template-stripped silver surface was easily damaged when sliding commenced. Only an estimate of S_c is given for this system. The other monolayers protected the silver surface much better and damage only appeared after prolonged sliding, as a small roughening of the surface (not the large failure commonly seen if a mica surface becomes damaged). ODT exhibited stick–slip sliding at the investigated sliding speeds and loads, shown as static (F_s) and kinetic friction (F_k) values in Figure 4d. The calculation of S_c for ODT is based on F_k. The other three systems occasionally showed stick–slip at the lowest loads, which changed into to smooth kinetic sliding after a few back-and-forth passes over the sliding range.

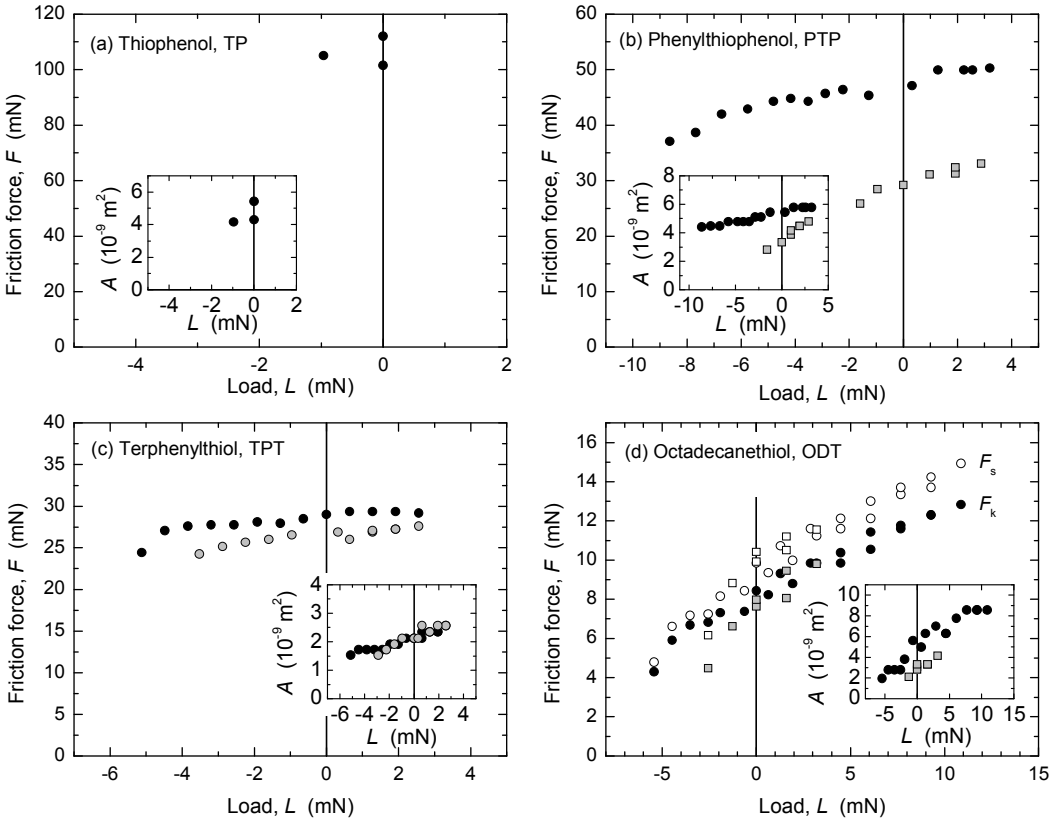

Figure 4. Friction force F vs. load L measured in dry N_2 with the SFA. Inserts: Measured nominal contact area A vs. L, used for calculation of $S_c = F/A$. (a) TP, $v \approx 3$ μm/s, R not measured. The TP-covered silver surface was easily damaged and only an estimate of S_c can be made for this system: $S_c \geq 20$ MPa. (b) PTP, (●) $v = 2.7$ μm/s, $R = 3.95$ cm, $S_c = 8.79$ MPa; (÷) $v = 3.2$ μm/s, $R = 2.57$ cm; $S_c = 7.8$ MPa. (c) TPT, two measurements on the same position with $v = 3.9$ μm/s, $R = 2.25$ cm, $S_c = 12.0$ and 13.9 MPa. (d) ODT, with the static and kinetic friction shown as open and closed symbols in the main panel. (○,●) $v = 3.2$ μm/s, R not measured, $S_c = 1.79$ MPa; (□,÷) $v \approx 3$ μm/s, $R = 2.9$ cm; $S_c = 3.3$ MPa.

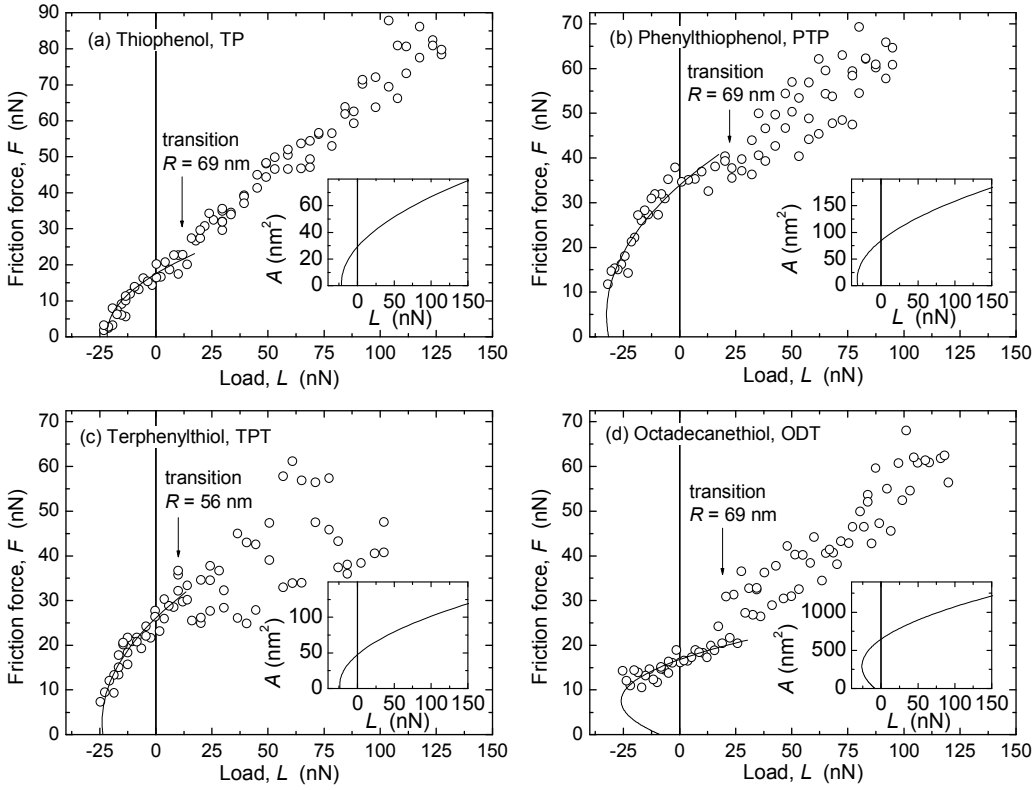

Figure 5. Friction force F vs. load L measured in dry N_2 with AFM. Scan velocity v = 2 μm/s. Inserts: Contact areas A calculated with the TCCM model, for determination of $S_c = F/A$. $F = S_cA$ curves are shown as solid lines in the main panels. (a) TP, R = 69 nm, E = 7 GPa, S_c = 600 MPa. (b) PTP, R = 69 nm, E = 3 GPa, S_c = 400 MPa. (c) TPT, R = 56 nm, E = 7 GPa, S_c = 550 MPa; (d) ODT, R = 69 nm, E = 0.2 GPa, S_c = 26 MPa.

AFM data from adhesive contacts cannot be analyzed in such a direct manner, since the nominal contact area cannot be directly measured. The solid curves in the main panels of Figures 5 are intended to describe the *low load* regime of the data only (below the transition regimes indicated by arrows), and represent $F = S_cA$, where S_c is a constant and the contact area A ($A = \pi a^2$) was calculated from a using a uniaxial elastic modulus of E_u = 15 GPa (E = 7 GPa, ν = 0.4) for the aromatic monolayers and E = 0.2 or 0.5 GPa (E_u = 0.4 or 1 GPa) for ODT. The resulting values of critical shear stress, S_c, from these and other experiments (cf. Supplementary Information) are summarized in Figure 6b and

Table 3. The highest friction is obtained with TP, and that of the more closely packed systems is lower. In each system, the interfacial energy γ_{TCCM} (= $W/2$) used in the calculated curves to reproduce the pull-off regime is in good agreement with the interfacial energy $\gamma_{vdW,AFM}$ calculated from bulk dielectric properties (Table 3).

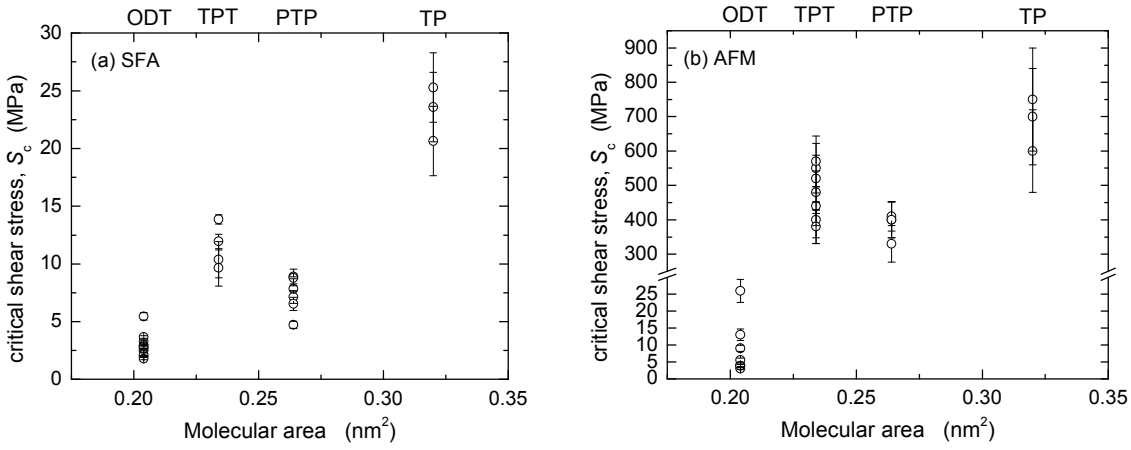

Figure 6. Critical shear stresses S_c for the four monolayer systems from (a) SFA and (b) AFM experiments in dry N_2.

DISCUSSION

SURFACE AND INTERFACIAL ENERGIES

The advancing and receding contact angles of water were similar on the PTP and TPT monolayers on silver, and slightly lower values were found for TP (Table 2). They were in good agreement with literature values in cases where these can be found[29,31,33,35] and similar to values obtained for these thiols on gold, where it has been concluded that the flat side of the terminal aromatic ring is partly accessible to the water.[9,10] The contact angle hysteresis ($\theta_{adv}-\theta_{rec} \approx 5°–20°$) was consistent with a similar chemical structure at the uppermost part of the three aromatic monolayers, and also similar to that found for these compounds on Au.

The experimental *surface* energy values γ_{YD} obtained from the contact angle

measurements were in good agreement with surface energies γ_{vdW} (Table 2) calculated using van der Waals–Lifshitz theory. Except for in the case of TP, there was also a good agreement between the *interfacial* energies γ_{TCCM} (=W/2), obtained from the comparison of curves calculated with the contact mechanics model to the pull-off region of AFM data (Figure 5) and the interfacial energies $\gamma_{vdW,AFM}$ calculated for the three-layer system SAM/N_2 gas/SiO_2 (Table 3). A similar calculation of interfacial energy can be done for the three-layer system SAM/ethanol/SiO_2, giving values of about 2 mJ/m^2, which is in good agreement with those obtained in the experiments in ethanol (cf. Results).

FRICTION MEASURED WITH THE SFA VERSUS THE AFM

An important issue in experiments with the SFA and AFM is the difference in contact area and pressure. Within the load range that can be conveniently reached in the SFA, the maximum pressure in the contact area is generally less than 50 MPa, whereas the contact pressures in the AFM, even at very low loads, are already close to the GPa range. In the very first systematic comparison of friction measurements with SFA and AFM, large differences were observed in the measured friction of confined polymer melts.[57] This was most likely due to different film thicknesses and AFM probe penetration of the confined films. One previous study has shown that quantitatively comparable friction results could be obtained with these techniques in *non-adhesive* systems where one or both surfaces were covered with a self-assembled aromatic silane monolayer,[18] as a way to provide a confined film (boundary lubricant layer) with similar thickness and structure in the different pressure ranges investigated.

The thiol monolayers in this study were chosen with this criterion in mind, and only the low-load data from AFM was evaluated, putting aside data from higher loads/different monolayer conformations expected after the monolayer transitions. Very similar values of the friction coefficients were consistently found with the two different methods for non-adhesive contact (Figure 1 and 2). There was a systematic decrease in μ with increasing packing density (Table 3), i.e., μ was highest for TP, and lower for PTP and TPT, but still higher than μ of close-packed ODT monolayers under similar conditions. The values were lower than those measured with AFM in systems where both surfaces

carried an aromatic thiol monolayer.[9]

Similar trends were found in the critical shear stresses, and within the accuracy of our experiments, S_c appeared to be a constant over the load range investigated in each experiment (for example, within each data set shown in Figures 4 and 5). However, a direct comparison between values obtained with the two techniques was complicated by the different methods by which the S_c values were obtained (from directly measured versus inferred contact areas where the choice of E strongly affects A and thus S_c), and by the observation of different results when a tip with much larger radius (R = 372 nm) was used for measurements on ODT (Figure 7) than that used in Figure 5d (69 nm).

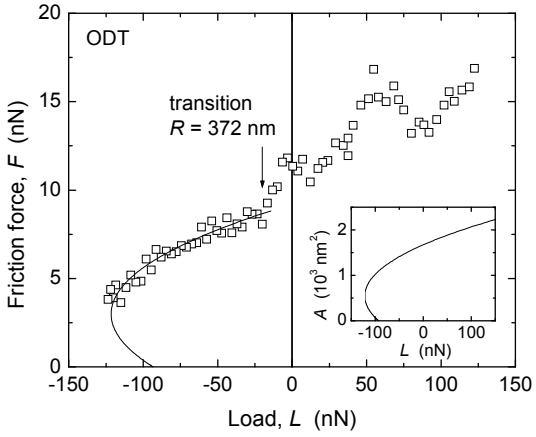

Figure 7. Friction force F vs. load L of ODT measured in dry N_2 with AFM. Scan velocity v = 2 μm/s. Insert: Contact area A calculated with the TCCM model. $F = S_cA$ is shown as a solid curve in the main panel. R = 372 nm, E = 0.5 GPa, S_c = 5.5 MPa.

When using R = 372 nm, a value of S_c = 5.1±1.1 MPa was found (cf. tabulated values in Supplementary Information), in closer agreement with the values measured with the SFA for ODT (2.9±0.3 MPa, Table 3) and other close-packed alkane-based systems.[20,58,59] In contrast, in AFM measurements in N_2 on aromatic thiols on gold, good agreement was found between S_c values obtained with R = 53–300 nm.[9] An important difference between these systems is the larger stiffness of the aromatic monolayers, as mentioned in the estimate of displacement in the section on the Contact Mechanics Model. The effects of different displacement or penetration with different techniques in films thinner and

stiffer than polymer melts (where this issue was first documented[57]) deserve further consideration.

SUMMARY

The Surface Forces Apparatus (SFA) technique and Atomic Force Microscopy (AFM) in friction mode were used to study the effects of adhesion strength and probe size on the friction forces in a series of self-assembled monolayer systems with different rigidity and packing density on silver substrates. A linear dependence of the friction force on load ($F = \mu L$) was found at low adhesion (measurements performed in ethanol). In the aromatic systems, μ was found to decrease with increasing packing density of the monolayers with both SFA and AFM. Higher adhesion (in N_2 gas) gave an apparent dependence on the nominal contact area of the form $F = S_c A$, where S_c is the critical shear stress. S_c can be calculated directly from the SFA data. In the cases of AFM, S_c values were obtained at low load in the adhesive systems by using the extended TCCM model for layered systems to calculate A vs. L. S_c was found to decrease with increasing molecular packing density. A Young's modulus of $E \approx 7$ GPa was needed to reproduce the F vs. L curves in these adhesive systems, whereas octadecanethiol (ODT) monolayers were described by $E \approx 0.2$ GPa and an S_c value closer to that obtained in the SFA experiments. Possible effects of displacement are discussed.

ACKNOWLEDGMENTS

The assistance of Jisun Im with XPS measurements is gratefully acknowledged. J. Mead is thanked for access to the contact angle analysis system and T. Pettersson is thanked for software to analyze the AFM data. This work was supported by NSF CAREER award CMMI-0645065 and through the NSF-funded Nanoscale Science and Engineering Center -- Center for High-Rate Nanomanufacturing (CHN) (award NSF-0425826).

SUPPLEMENTARY INFORMATION

Calculation of surface energy. Friction coefficients. Critical shear stresses.

REFERENCES

1. J. N. Israelachvili and A. D. Berman, in *Handbook of Micro/Nanotribology, 2nd ed*., ed. B. Bhushan, CRC Press, Boca Raton, FL, 1999, p. 371–432
2. R. W. Carpick and M. Salmeron, *Chem. Rev.*, 1997, **97**, 1163–1194.
3. R. W. Carpick, N. Agraït, D. F. Ogletree and M. Salmeron, *Langmuir*, 1996, **12**, 3334–3340.
4. G. Bogdanovic, F. Tiberg and M. W. Rutland, *Langmuir*, 2001, **17**, 5911–5916.
5. S. Ecke and H.-J. Butt, *J. Colloid Interface Sci.*, 2001, **244**, 432–435.
6. C. R. Hurley and G. J. Leggett, *Langmuir*, 2006, **22**, 4179–4183.
7. T. J. Colburn and G. J. Leggett, *Langmuir*, 2007, **23**, 4959–4964.
8. M. Ruths, S. Lundgren, K. Danerlöv and K. Persson, *Langmuir*, 2008, **24**, 1509–1516.
9. Y. Yang and M. Ruths, *Langmuir*, 2009, **25**, 12151–12159.
10. Y. Yang, A. C. Jamison, D. Barriet, T. R. Lee and M. Ruths, *J. Adh. Sci. Techn*. 2010, **24**, 2511–2529.
11. K. Busuttil, N. Nikogeorgos, Z. Zhang, M. Geoghegan, C. A. Hunter and G. J. Leggett. *Faraday Disc.* 2012, **156**, 325–341.
12. N. Nikogeorgos, C. A. Hunter and G. J. Leggett. *Langmuir*, 2012, **28**, 17709–17717.
13. K. L. Johnson, K. Kendall and A. D. Roberts, *Proc. R. Soc. Lond. A*, 1971, **324**, 301–313.
14. B.V. Derjaguin, V. M. Muller, Yu. P. Toporov, *J. Colloid Interface Sci*., 1975, **53**, 314–326.
15. R. W. Carpick, D. F. Ogletree, M. Salmeron, *J. Colloid Interface Sci*., 1999, **211**, 395–400.
16. M. Ruths, *J. Phys. Chem. B*, 2006, **110**, 2209–2218.
17. A. Berman, C. Drummond and J. Israelachvili, *Trib. Lett*., 1998, **4**, 95–101.
18. M. Ruths, N. A. Alcantar and J. N. Israelachvili, *J. Phys. Chem. B*, 2003, **107**, 11149–11157.
19. M. Ruths, *Langmuir*, 2003, **19**, 6788–6795.

20. M. Ruths and J. N. Israelachvili, in *Springer Handbook of Nanotechnology, 3rd ed*., ed. B. Bhushan, Springer-Verlag, Berlin & Heidelberg, 2010, p. 857–922.
21. Y. Mo, K. T. Turner, I. Szlufarska, *Nature*, 2009, **457**, 1116–1119.
22. Y. Mo and I. Szlufarska, *Phys. Rev. B,* 2010, **81**, 035405/1–17.
23. S. Cheng, B. Luan and M. Robbins, *Phys. Rev. E*, 2010, **81**, 016102/1–17.
24. B. Luan and M. O. Robbins, *Nature*, 2005, **435**, 929–932.
25. M. Salmeron, *Trib. Lett*., 2001, **10**, 69–79.
26. P. T. Mikulski and J. A. Harrison, *J. Am. Chem. Soc*., 2001, **123**, 6873–6881.
27. B. Bhushan and H. Liu, *Phys. Rev. B*, 2001, **63**, 245412/1–11.
28. S. Lee, Y.-S. Shon, R. Colorado, Jr., R. L. Guenard, T. R. Lee and S. S. Perry, *Langmuir*, 2000, **16**, 2220–2224.
29. J. Y. Gui, D. A. Stern, D. G. Frank, F. Lu, D. C. Zapien, and A. T. Hubbard, *Langmuir*, 1991, **7**, 955–963.
30. M. C. Schalnat and J. E. Pemberton, *Langmuir*, 2010, **26**, 11862–11869.
31. S. Frey, V. Stadler, K. Heister, W. Eck, M. Zharnikov, and M. Grunze, *Langmuir*, 2001, **17**, 2408–2415.
32. A. A. Mani, Z. D. Schultz, B. Champagne, C. Humbert, L. Dreesen, A. A. Gewirth, J. O. White, P. A. Thiry, A. Peremans, and Y. Caudano, *Appl. Surf. Sci*., 2004, **237**, 444–449.
33. A. Shaporenko, A. Terfort, M. Grunze and M. Zharnikov, *J. Electr. Spectr. Rel. Phenom*., 2006, **151**, 45–51.
34. U. Weckenmann, S. Mittler, K. Naumann, and R. A. Fischer, *Langmuir*, 2002, **18**, 5479–5486.
35. A. Shaporenko, M. Brunnbauer, A. Terfort, M. Grunze and M. Zharnikov, *J. Phys. Chem. B*, 2004, **108**, 14462–14469.
36. P. E. Laibinis, G. M. Whitesides, D. L. Allara, Y.-T. Tao, A. N. Parikh, and R. G. Nuzzo, *J. Am. Chem. Soc*., 1991, **113**, 7152–7167.

37. J. P. Folkers, J. A. Zerkowski, P. E. Laibinis, C. T. Seto, G. M. Whitesides, in *ACS Symposium Series No. 499*, ed. T. Bein, American Chemical Society, Washington, DC, 1992, p. 10–23.
38. Y.-T. Tao, C.-C. Wu, J.-Y. Eu, W.-L. Lin, K.-C. Wu, C.-h. Chen, *Langmuir* 1997, **13**, 4018–4023.
39. H. H. Jung, Y. D. Won, S. Shin, K. Kim, *Langmuir*, 1999, **15**, 1147–1154.
40. J. N. Israelachvili, *Intermolecular and Surface Forces*, 3rd ed., Elsevier, Amsterdam, 2011.
41. H. Y. Erbil, *Surface Chemistry of Solid and Liquid Interfaces*. Blackwell, Oxford, 2006.
42. J. N. Israelachvili, G. E. Adams, *J. Chem. Soc., Faraday Trans. 1*, 1978, **74**, 975–1001.
43. J. N. Israelachvili, *J. Colloid Interface Sci*., 1973, **44**, 259–272.
44. I. Sridhar, K. L. Johnson and N. A. Fleck, *J. Phys. D.: Appl. Phys*. 1997, **30**, 1710–1719.
45. J. N. Israelachvili and P. M. McGuiggan, *J. Mater. Res*., 1990, **5**, 2223–2231.
46. G. Luengo, F.-J. Schmitt, R. Hill and J. N. Israelachvili, *Macromolecules*, 1997, **30**, 2482–2492.
47. J. E. Sader, J. W. M. Chon and P. Mulvaney, *Rev. Sci. Instrum*., 1999, **70**, 3967–3969.
48. C. P. Green, H. Lioe, J. P. Cleveland, R. Proksch, P. Mulvaney and J. E. Sader, *Rev. Sci. Instrum*., 2004, **75**, 1988–1996.
49. Y. Liu, T. Wu and D. F. Evans, *Langmuir*, 1994, **10**, 2241– 2245.
50. Y. Liu, D. F. Evans, Q. Song and D. W. Grainger, *Langmuir*, 1996, **12**, 1235–1244.
51. H. K. Christenson, *Langmuir*, 1996, **12**, 1404–1405.
52. R. G. Munro, *Elastic Moduli Data for Polycrystalline Oxide Ceramics*, NISTIR 6853, National Institute of Standards and Technology, Gaithersburg, Maryland, 2002.
53. E. D. Reedy, Jr., *J. Mater. Res*., 2006, **21**, 2660–2668.
54. E. D. Reedy, Jr., *J. Mater. Res*., 2007, **22**, 2617–2622.

55. E. D. Reedy, Jr., M. J. Starr, R. E. Jones, E. E. Flater and R. W. Carpick, in *Proceedings of the 28th Annual Meeting of the Adhesion Society*, Mobile, AL, 2005, p. 366–368.
56. M. Chandross, C. D. Lorenz, M. J. Stevens and G. S. Grest, *Langmuir*, 2008, **24**, 1240.
57. P. M. McGuiggan, J. Zhang and S. M. Hsu, *Tribol. Lett*., 2001, **10**, 217–223.
58. A. I. Bailey and J. S. Courtney-Pratt, *Proc. Roy. Soc. Lond. A*, 1955, **227** 500–515.
59. B. J. Briscoe and D. C. B. Evans, *Proc. Roy. Soc. Lond. A*, 1982, **380**, 389–407.

Table of Contents entry:

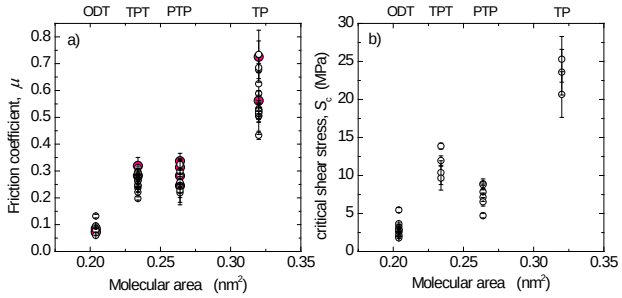

(a) Friction coefficients and (b) critical shear stresses of thiol monolayers on silver, measured with SFA (○) and AFM (red circles).